Kirchhoff prestack depth migration in a homogeneous triclinic velocity model for P, S and converted waves

Václav Bucha
Department of Geophysics, Faculty of Mathematics and Physics, Charles University in Prague, Ke Karlovu 3, 121 16 Praha 2, Czech Republic, bucha@seis.karlov.mff.cuni.cz

Summary

The ray-based Kirchhoff prestack depth migration is used to calculate migrated sections in a simple homogeneous triclinic velocity model. The ray-theory recorded wave field corresponding to P, S and converted waves is generated in the velocity model composed of two homogeneous layers separated by a non-inclined curved interface. The anisotropy of the upper layer is triclinic. We apply the Kirchhoff prestack depth migration to single-layer velocity model with the same triclinic anisotropy as in the upper layer of the velocity model used to calculate the recorded wave field. We show and discuss the results of the migration for different types of waves.

Keywords

3-D Kirchhoff prestack depth migration, anisotropic velocity model, triclinic anisotropy

1. Introduction

We continue in the ray-based Kirchhoff prestack depth migration studies. While the previous studies were limited to P waves, in this paper we use also ray-theory S waves and converted waves. The dimensions of the velocity model, shot-receiver configuration, methods for calculation of the recorded wave field and the migration are the same as in the previous papers by Bucha (e.g., 2012, 2013, 2014), where we studied the sensitivity of the migrated images to incorrect anisotropy, to incorrect gradients of elastic moduli or to incorrect rotation of the tensor of elastic moduli.

We generate synthetic seismograms of reflected P, S and converted waves using the ray theory which is approximate. We consider only vertical components. To compute the synthetic recorded wave field, we use simple anisotropic velocity model composed of two homogeneous layers separated by one curved interface that is non-inclined in the direction perpendicular to the source-receiver profiles. The anisotropy in the upper layer is triclinic and is thus not mirror symmetric. The complexity of the anisotropy is obvious from the generated and displayed ray-velocity surfaces of P, S1 and S2 waves.

We then migrate the synthetic data using the 3-D ray-based Kirchhoff prestack depth migration in the correct single-layer triclinic velocity model. The elastic moduli in the correct velocity model correspond to the upper layer of the velocity model in which the synthetic seismograms have been calculated.

Seismic Waves in Complex 3–D Structures, **25** (2015), 89–102 (ISSN 2336–3827, online at http://sw3d.cz)

2. Anisotropic velocity model

The dimensions of the velocity model and the measurement configuration are derived from the 2-D Marmousi model and dataset (Versteeg & Grau, 1991). The horizontal dimensions of the velocity model are $0\ km \leq x_1 \leq 9.2\ km$, $0\ km \leq x_2 \leq 10\ km$ and the depth is $0\ km \leq x_3 \leq 3\ km$. The velocity model is composed of two layers separated by one non-inclined curved interface (see Figure 1). The curved interface is non-inclined in the direction of the x_2 axis which is perpendicular to the source-receiver profiles.

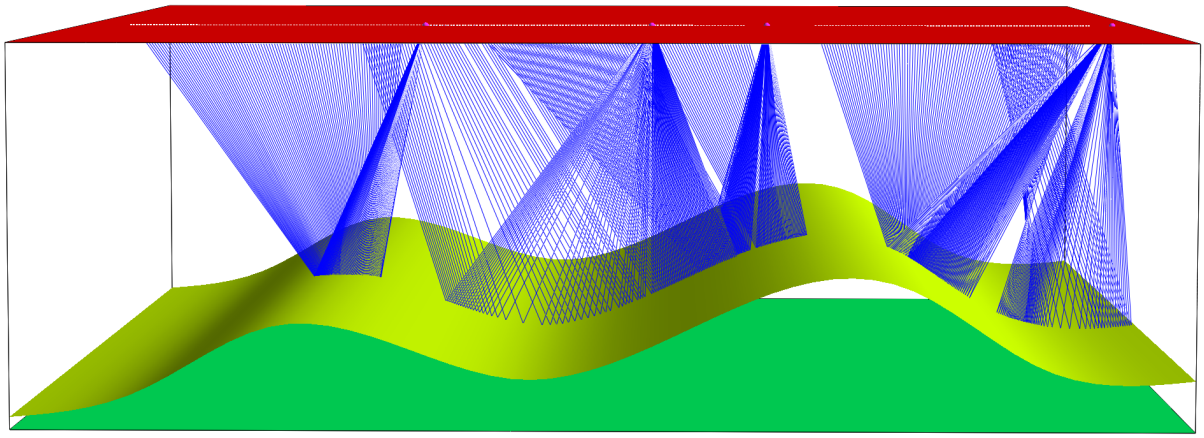

Figure 1. Velocity model with a non-inclined curved interface and with triclinic anisotropy in the upper layer. The horizontal dimensions of the velocity model are $0\ km \leq x_1 \leq 9.2\ km$, $0\ km \leq x_2 \leq 10\ km$ and the depth is $0\ km \leq x_3 \leq 3\ km$. The velocity model contains one curved interface which is non-inclined in the direction perpendicular to the source-receiver profiles. Two-point rays of the converted PS2 wave for one selected profile line (at horizontal coordinate $x_2 = 6$ km) and four shot-receiver configurations (shots 1, 80, 120 and 240 along the profile) are displayed.

The recorded wave field is computed in the velocity model composed of two homogeneous layers. The medium in the upper layer of the velocity model is triclinic. The bottom layer is isotropic.

The triclinic medium is represented by dry Vosges sandstone (Mensch & Rasolofosaon, 1997). Triclinic anisotropy is asymmetric. The matrix of density-reduced elastic moduli in km^2/s^2 reads

$$\begin{pmatrix} 10.3 & 0.9 & 1.3 & 1.4 & 1.1 & 0.8 \\ & 10.6 & 2.1 & 0.2 & -0.2 & -0.6 \\ & & 14.1 & 0.0 & -0.5 & -1.0 \\ & & & 5.1 & 0.0 & 0.2 \\ & & & & 6.0 & 0.0 \\ & & & & & 4.9 \end{pmatrix}. \tag{1}$$

We migrate in the correct single-layer velocity model (without the curved interface) with the same triclinic anisotropy given by matrix (1). The elastic moduli in the correct velocity model correspond to the upper layer of the velocity model in which the synthetic data have been calculated.

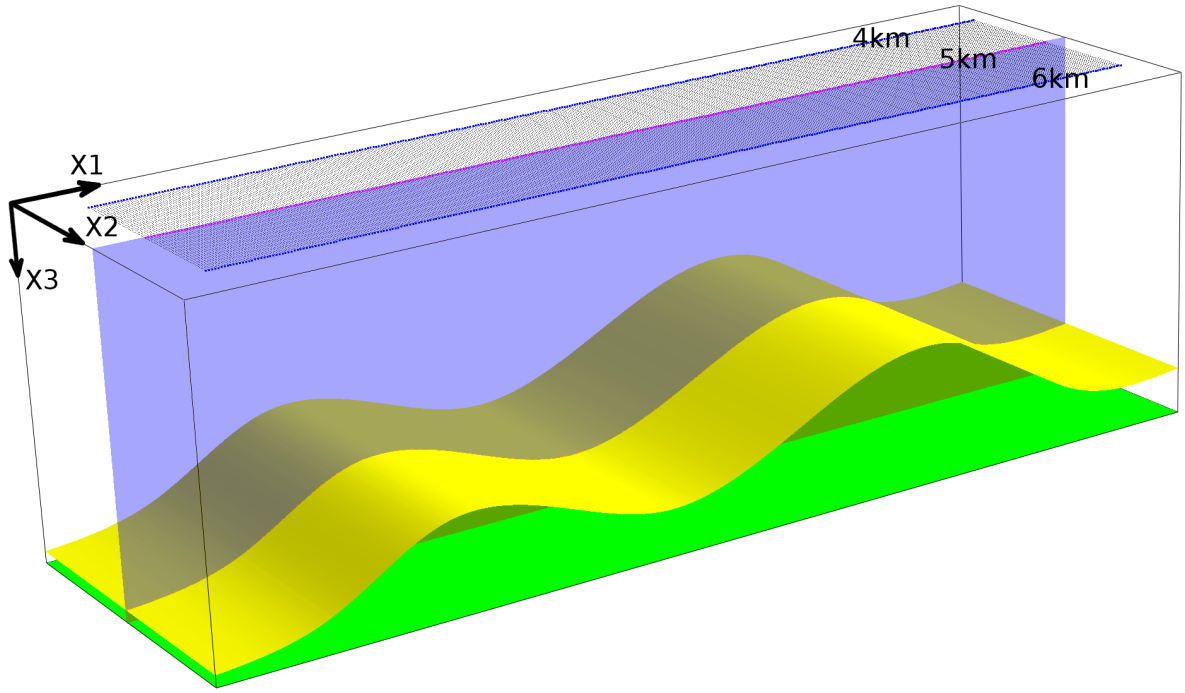

Figure 2. Part of the velocity model with 81 parallel profile lines, the non-inclined curved interface (yellow) and the bottom velocity model plane (green). The horizontal dimensions of the depicted part of the velocity model are $0\ km \leq x_1 \leq 9.2\ km$, $3.5\ km \leq x_2 \leq 6.5\ km$, the depth is $0\ km \leq x_3 \leq 3\ km$. We compute and stack migrated sections in the 2-D plane (blue) located in the middle of the shot-receiver configuration, at horizontal coordinate $x_2 = 5\ km$.

3. Shots and receivers

The measurement configuration is derived from the Marmousi model and dataset (Versteeg & Grau, 1991). The profile lines are parallel with the x_1 coordinate axis. Each profile line has the following configuration: The first shot is 3 km from the left-hand side of the velocity model, the last shot is 8.975 km from the left-hand side of the velocity model (see Figure 1), the distance between the shots is 0.025 km, and the depth of the shots is 0 km. The total number of shots along one profile line is 240. The number of receivers per shot is 96, the first receiver is located 2.575 km left of the shot location, the last receiver is 0.2 km left of the shot location, the distance between the receivers is 0.025 km, and the depth of the receivers is 0 km. This configuration simulates a simplified towed streamed acquisition geometry.

The 3-D measurement configuration consists of 81 parallel profile lines, see Figure 2. The interval between the parallel profile lines is 0.025 km.

4. Recorded wave field

The recorded wave field in the triclinic velocity model was computed using the ANRAY software package (Gajewski & Pšenčík, 1990). 3-D ray tracing is used to calculate the two-point rays of the reflected P, S and converted waves. We then compute the ray-theory seismograms at the receivers. Calculations are limited to vertical component.

The recorded wave field is equal for all parallel profile lines, because the distribution of elastic moduli in each layer is homogeneous, and the non-inclined curved interface is independent of the coordinate x_2 perpendicular to the profile lines (2.5-D velocity model, see Figures 1 and 2).

The triclinic asymmetry causes that the two-point rays do not stay in the vertical planes corresponding to the individual profiles (see Figure 3).

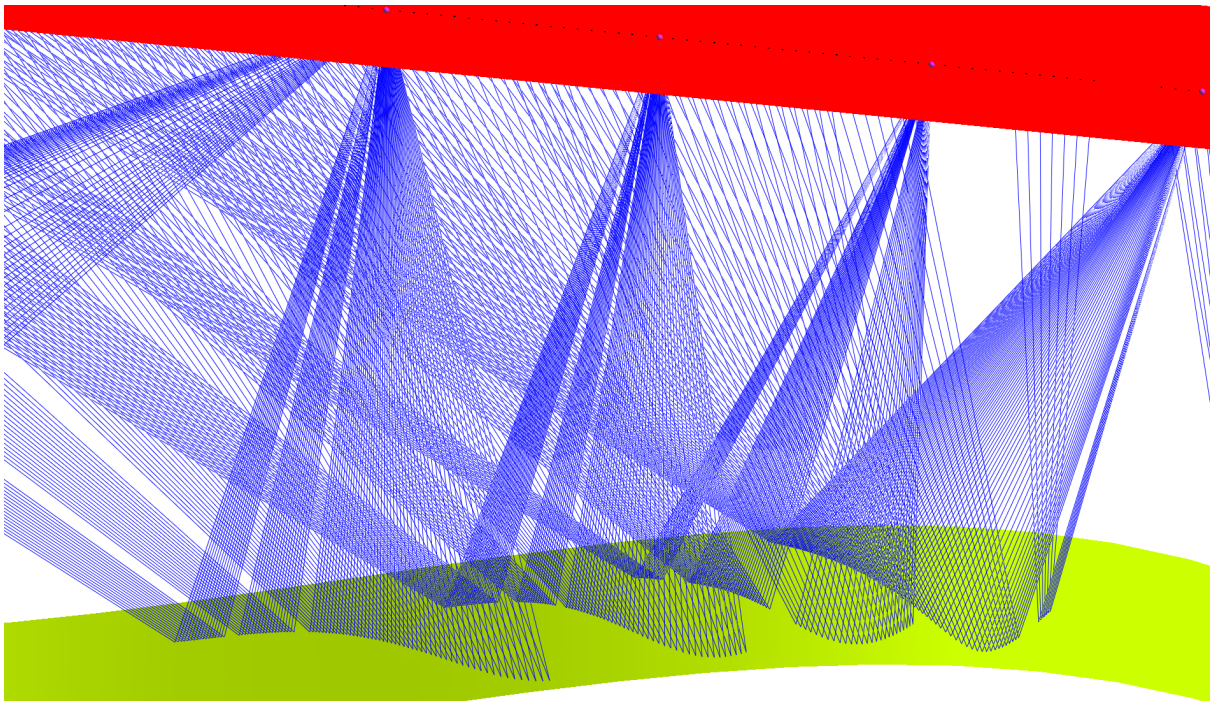

Figure 3. Detailed view of two-point rays of the reflected S1S2 wave for shots 80, 100, 120 and 140. Note the curved paths of reflections at the interface.

4.1 Ray-velocity surfaces

To see how problematic is calculating ray-theory S waves, we generate and display the ray-velocity surfaces for the relatively strong triclinic anisotropy (1). The ray-velocity surface (group-velocity surface, Fresnel wave surface) at spatial point x^m is composed of three sheets corresponding to the three eigenvalues of the Christoffel matrix (Klimeš, 2002).

While the ray-velocity surface of the P wave is convex and smooth (see Figure 4), the surfaces of the ray-theory S1 and S2 waves are much more complex (see Figures 5-12). The detailed study of S1 and S2 surfaces shows many common, singular points. Some parts of the ray-velocity S1 and S2 surfaces are concave or intersect. All these anomalies cause calculation problems in some directions.

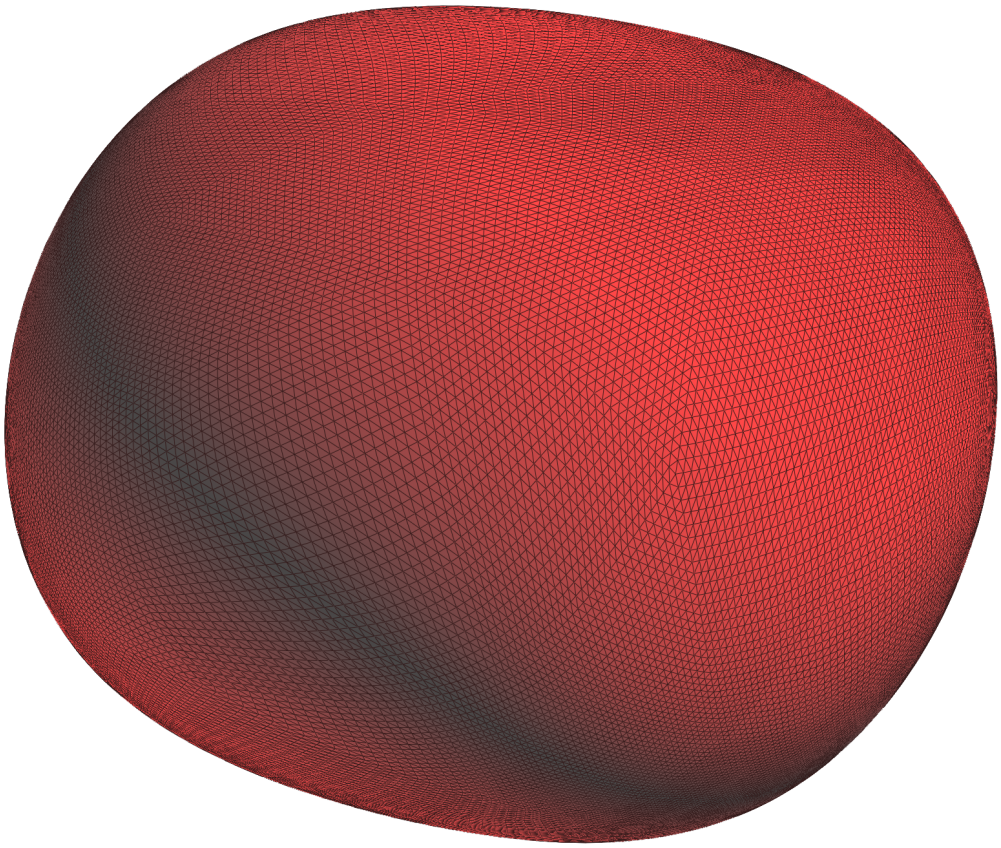

Figure 4. The **P** ray-velocity surface for the triclinic anisotropy.

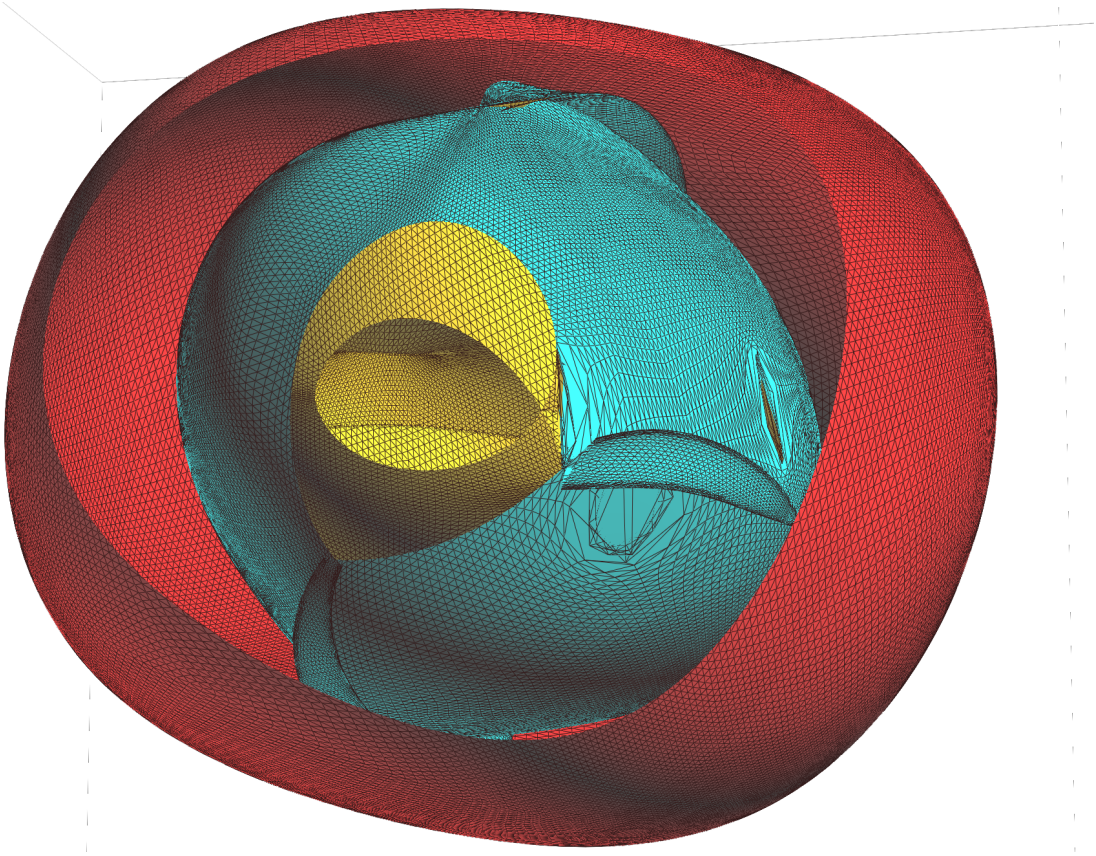

Figure 5. The sliced **P**, **S1** and **S2** ray-velocity surfaces for the triclinic anisotropy.

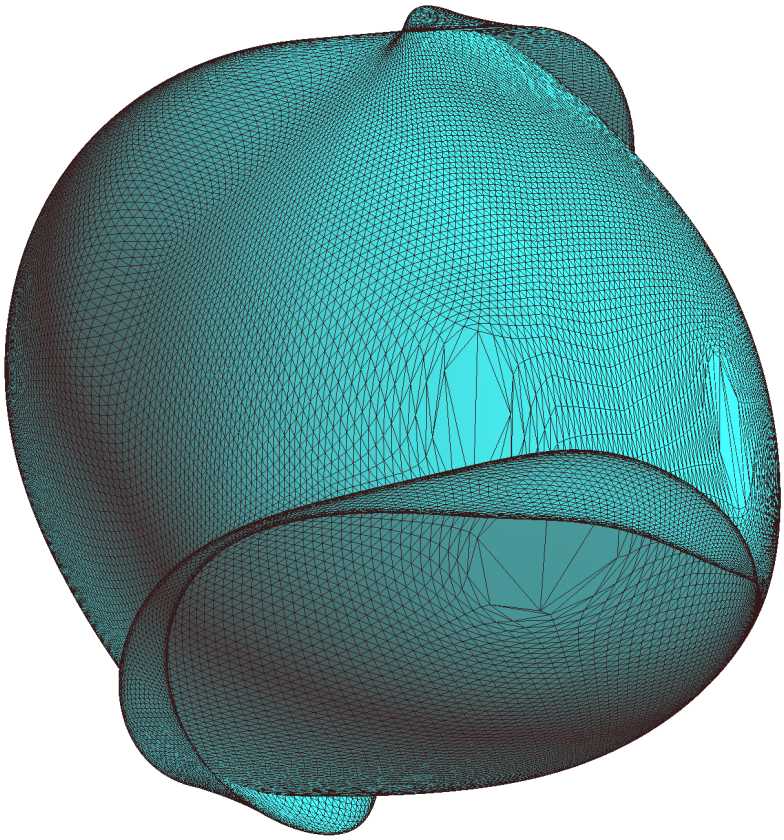

Figure 6. The S2 ray-velocity surface for the triclinic anisotropy.

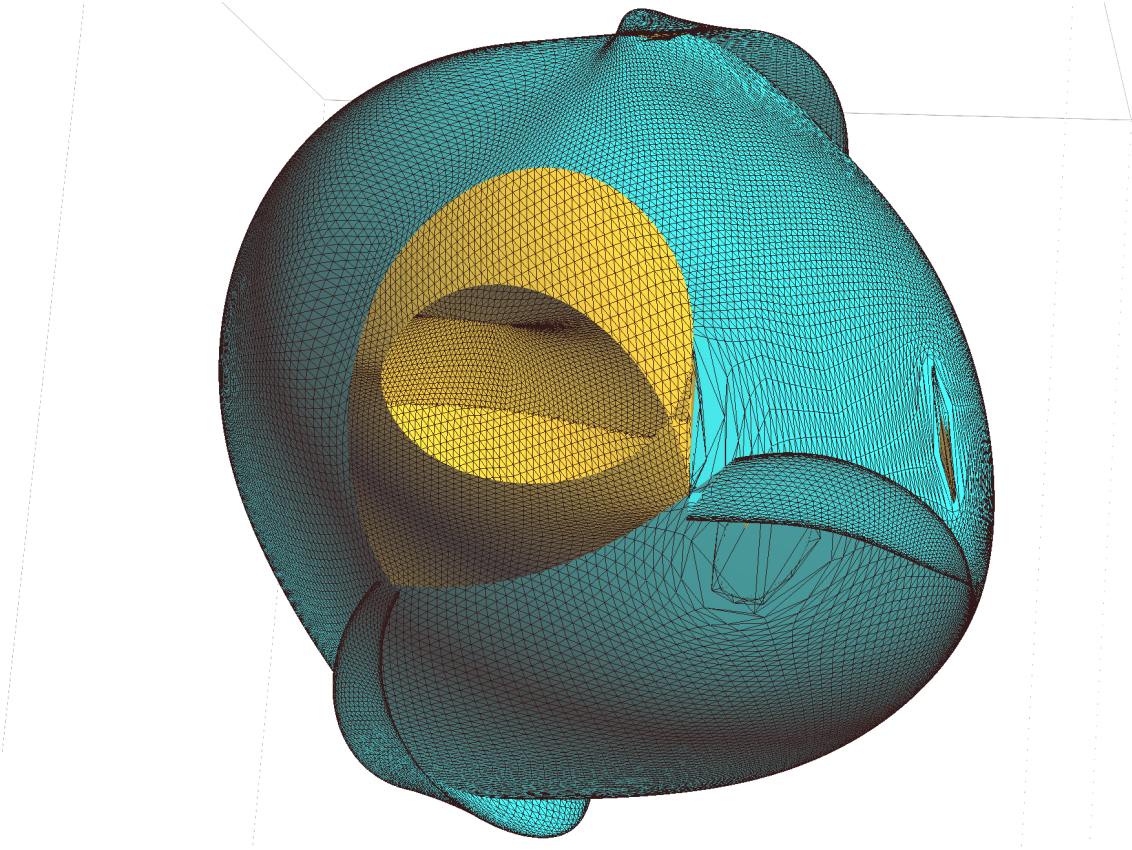

Figure 7. The sliced S1 and S2 ray-velocity surfaces for triclinic anisotropy.

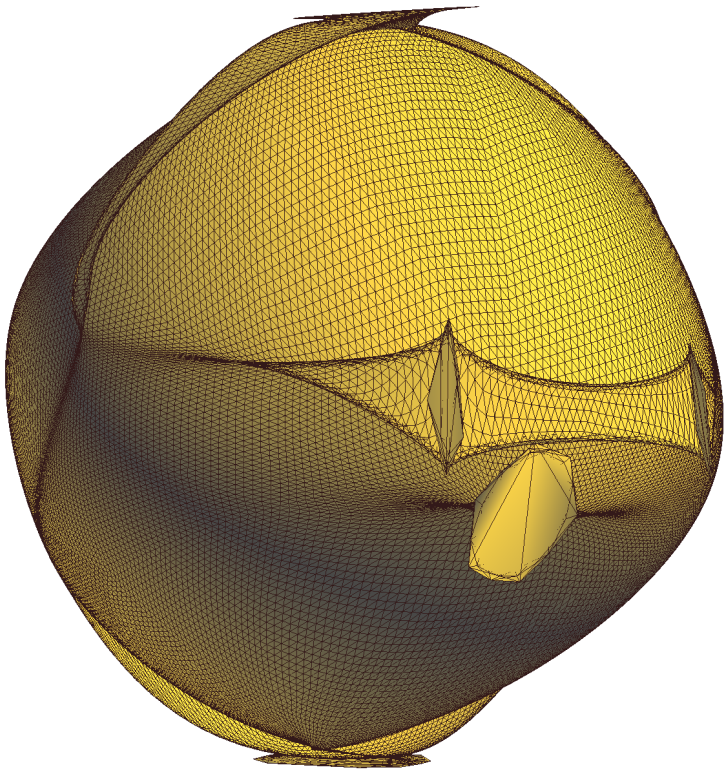

Figure 8. The S1 ray-velocity surface for the triclinic anisotropy.

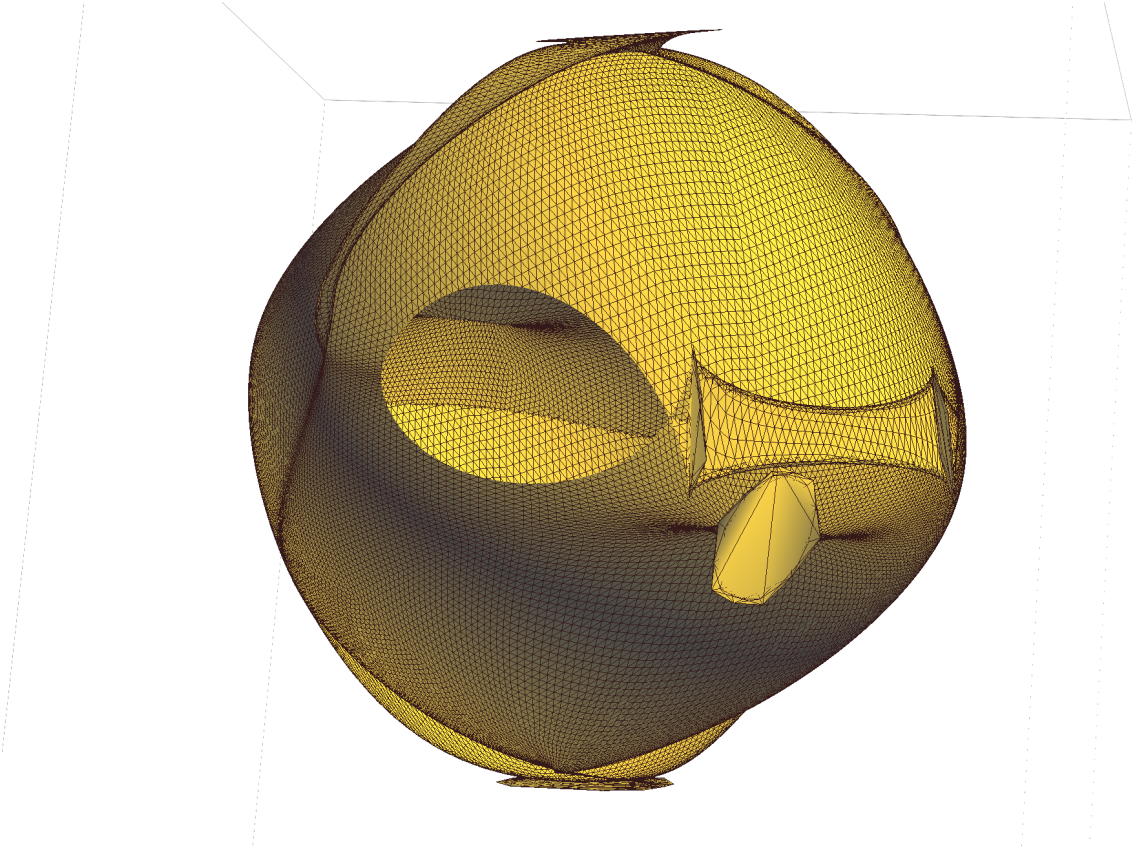

Figure 9. The sliced S1 ray-velocity surface for the triclinic anisotropy.

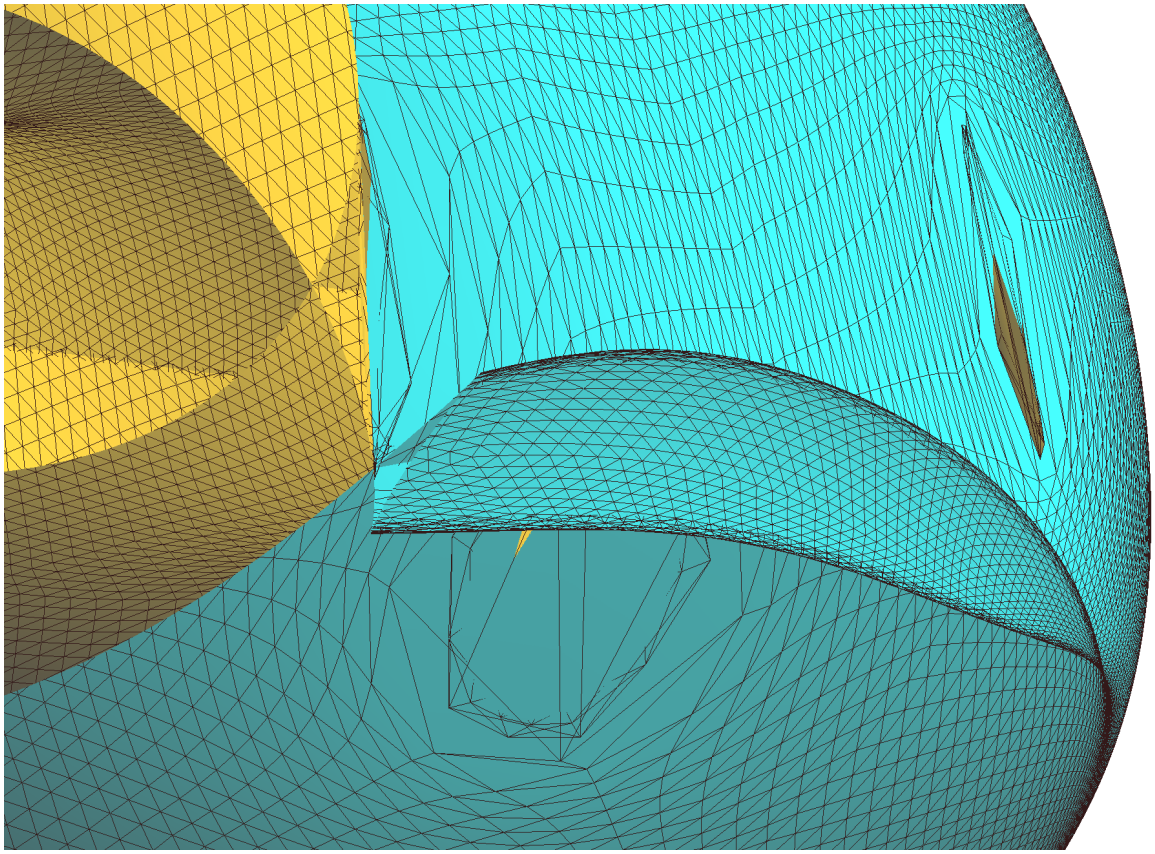

Figure 10. Detail of the sliced S1 and S2 ray-velocity surfaces for the triclinic anisotropy.

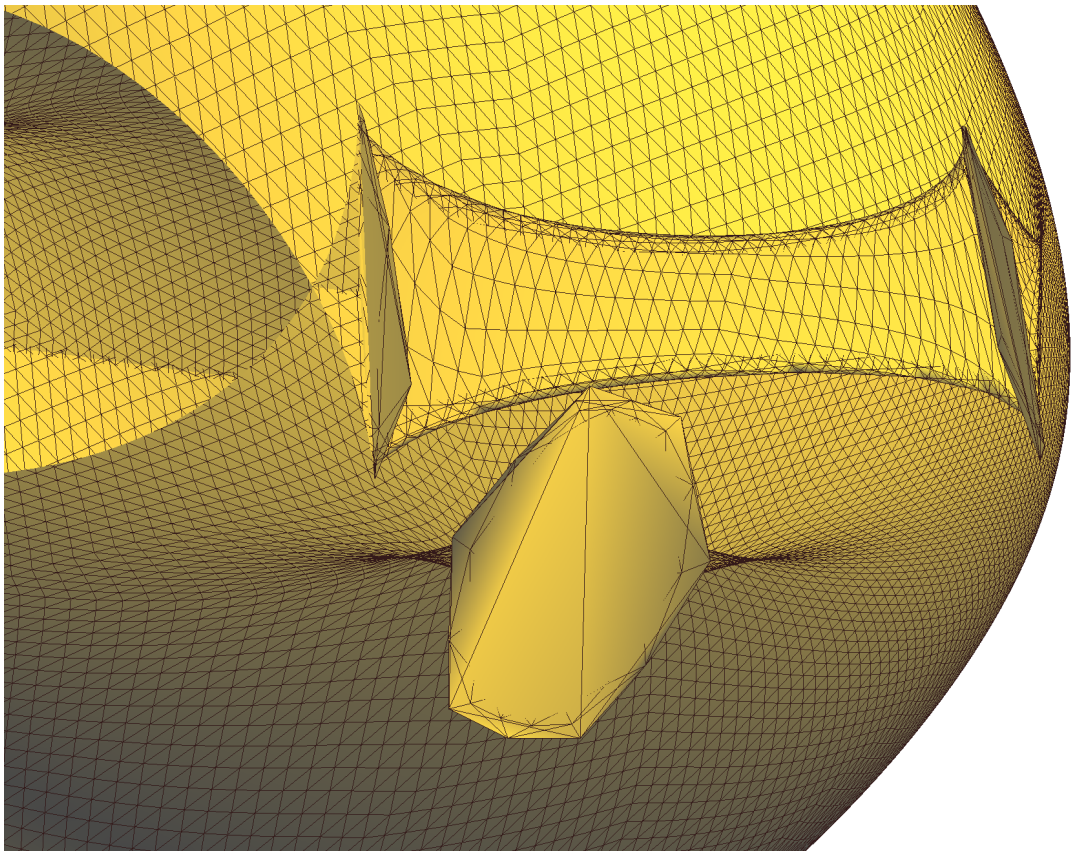

Figure 11. Detail of the sliced S1 ray-velocity surface for the triclinic anisotropy.

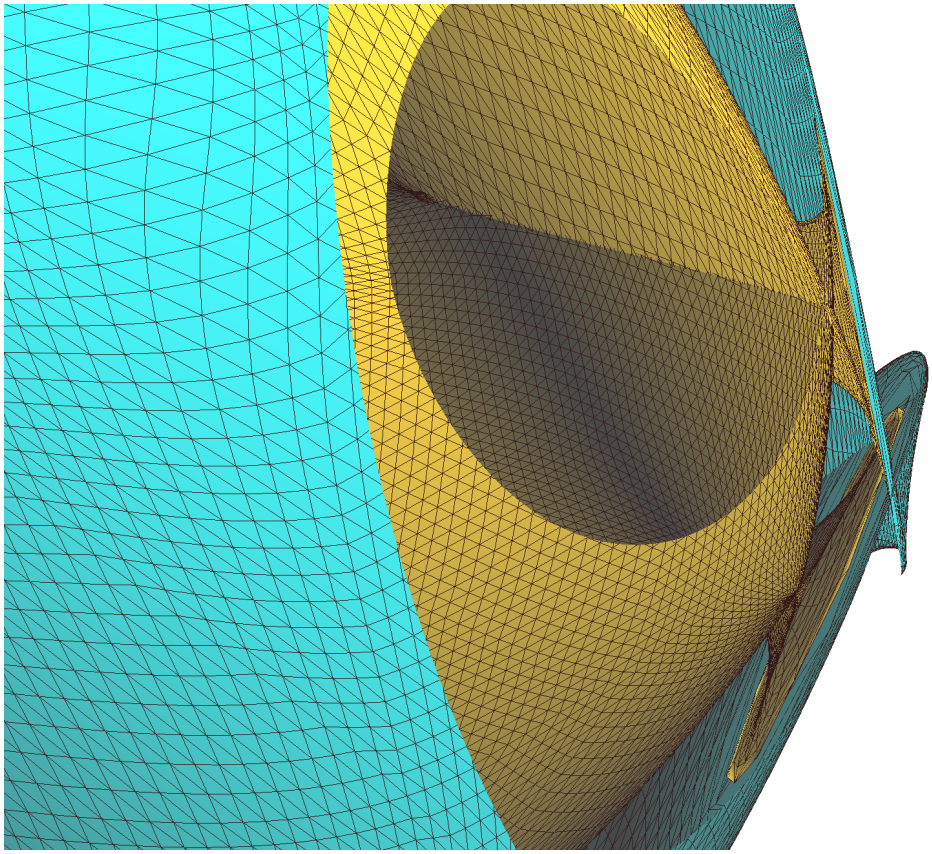

Figure 12. Detail of the sliced S1 and S2 ray-velocity surfaces for the triclinic anisotropy.

4.2 Synthetic seismograms

For S and converted waves, we observe seismograms with enormous amplitudes for some shot-receiver configurations, caused probably by singularities. On the other side, we observe receivers with no or very small amplitudes. The reason is that we calculate only vertical component, or that two-point rays were not computed in some directions. Seismograms and migration should be completed by radial and transversal components in future.

Figure 13 shows vertical components of the seismograms for 9 elementary reflected waves for a selected shot-receiver configuration: PP wave, PS2 wave, PS1 wave, S2P wave, S1P wave, S2S2 wave, S1S2 wave, S2S1 wave and S1S1 wave. Notation is simple, the first letter denotes elementary wave from the source to the reflection point and the second letter denotes elementary wave from the reflection point to the receiver. P is for P wave, S1 and S2 are for ray-theory S waves.

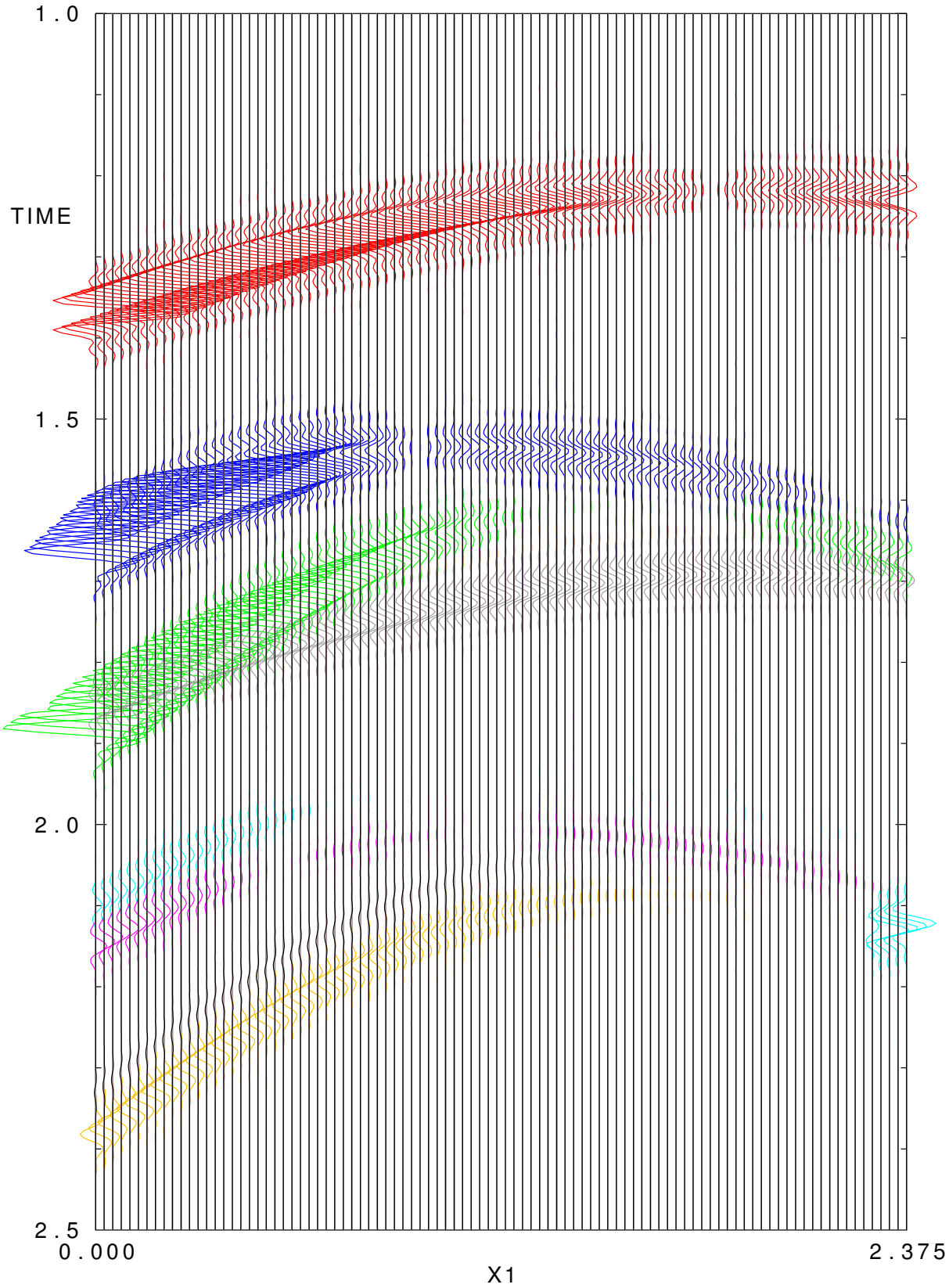

Figure 13. Vertical component of the synthetic seismograms of the reflected P, S and converted waves for the single common-shot gather at line $x_2 = 5$ km corresponding to shot 20 ($x_1 = 3.475$ km). The 9 elementary waves, ordered approximately according to travel time from the smallest, are **PP** wave, **PS2** wave, **PS1** wave, **S2P** wave (nearly invisible), **S1P** wave, **S2S2** wave, **S1S2** wave, **S2S1** wave (poorly visible) and **S1S1** wave. All seismograms have the same scaling.

5. Kirchhoff prestack depth migration

We use the MODEL, CRT, FORMS and DATA packages for the 3-D Kirchhoff prestack depth migration (Červený, Klimeš & Pšenčík, 1988; Bulant, 1996; Bucha & Bulant, 2015). The migration consists of two-parametric controlled initial-value ray tracing (Bulant, 1999) from the individual surface points, calculating grid values of travel times and amplitudes by interpolation within ray cells (Bulant & Klimeš, 1999), performing the common-shot migration and stacking the migrated images. The shot-receiver configuration consists of 81 parallel profile lines at intervals of 0.025 km (see Figure 2). The first profile line is situated at horizontal coordinate $x_2 = 4$ km and the last profile line is situated at horizontal coordinate $x_2 = 6$ km. For migration we use the single-layer velocity model (without the curved interface).

The elastic moduli in the single-layer velocity model for migration are the same as in the upper layer of the velocity model used to calculate the recorded wave field (matrix (1)).

Figure 14 shows the stacked migrated section calculated for the reflected PP wave using only the vertical components of the seismograms. This calculation was done earlier and was presented e.g., in Bucha (2012). The migrated interface is clear and coincides nearly perfectly with the interface in the velocity model used to compute the recorded wave field.

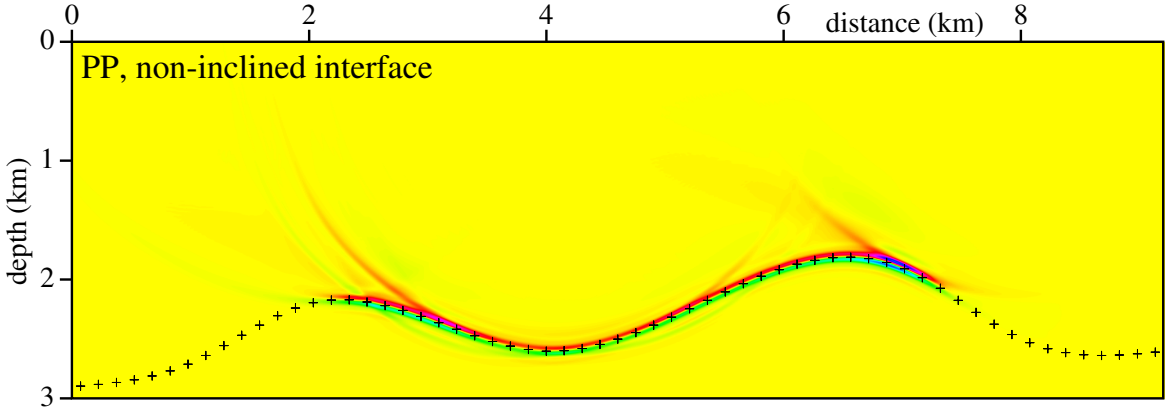

Figure 14. Stacked migrated sections calculated in the correct velocity model without interfaces specified by triclinic anisotropy. The PP reflected wave is used. The elastic moduli in the single-layer velocity model for migration are the same as in the upper layer of the velocity model used to calculate the recorded wave field. 81 × 240 common-shot prestack depth migrated sections, corresponding to 81 profile lines and 240 sources along each profile line, have been stacked. The crosses denote the interface in the velocity model used to compute the recorded wave field.

Figure 15 shows the stacked migrated sections calculated for the reflected ray-theory S1S1, S2S2, S1S2 and S2S1 elementary waves using only the vertical components of the seismograms. Some parts of migrated sections are poorly imaged and are much more noisy than the PP wave migrated section (Figure 14). Note reverse amplitudes for S1S1, S1S2 compared with S2S2, S2S1 (red and green colours). The summation of all four sections thus might diminish the result. During calculations, we encounter problems with anomalous amplitudes of the Green function caused by singularities.

Figure 16 shows the stacked migrated sections calculated for the converted PS1, PS2, S1P and S2P elementary waves using only the vertical components of the seismograms. Similarly as for the reflected S wave, some parts of the migrated sections are poorly imaged and are noisy.

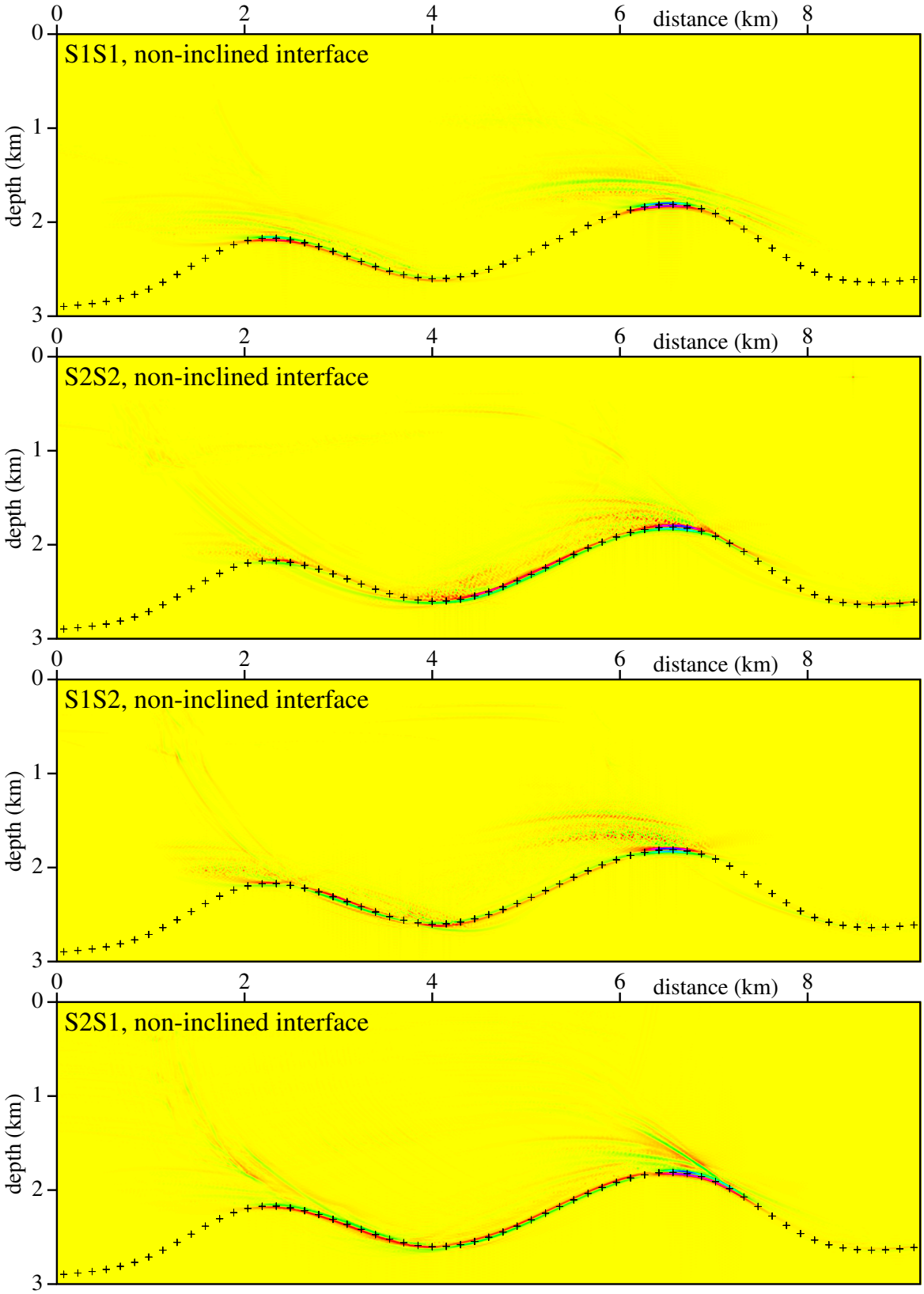

Figure 15. Stacked migrated sections calculated in the correct velocity model without interfaces specified by triclinic anisotropy. The S1S1, S2S2, S1S2 and S2S1 reflected waves are used. The elastic moduli in the single-layer velocity model for migration are the same as in the upper layer of the velocity model used to calculate the recorded wave field. 81×240 common-shot prestack depth migrated sections, corresponding to 81 profile lines and 240 sources along each profile line, have been stacked. The crosses denote the interface in the velocity model used to compute the recorded wave field.

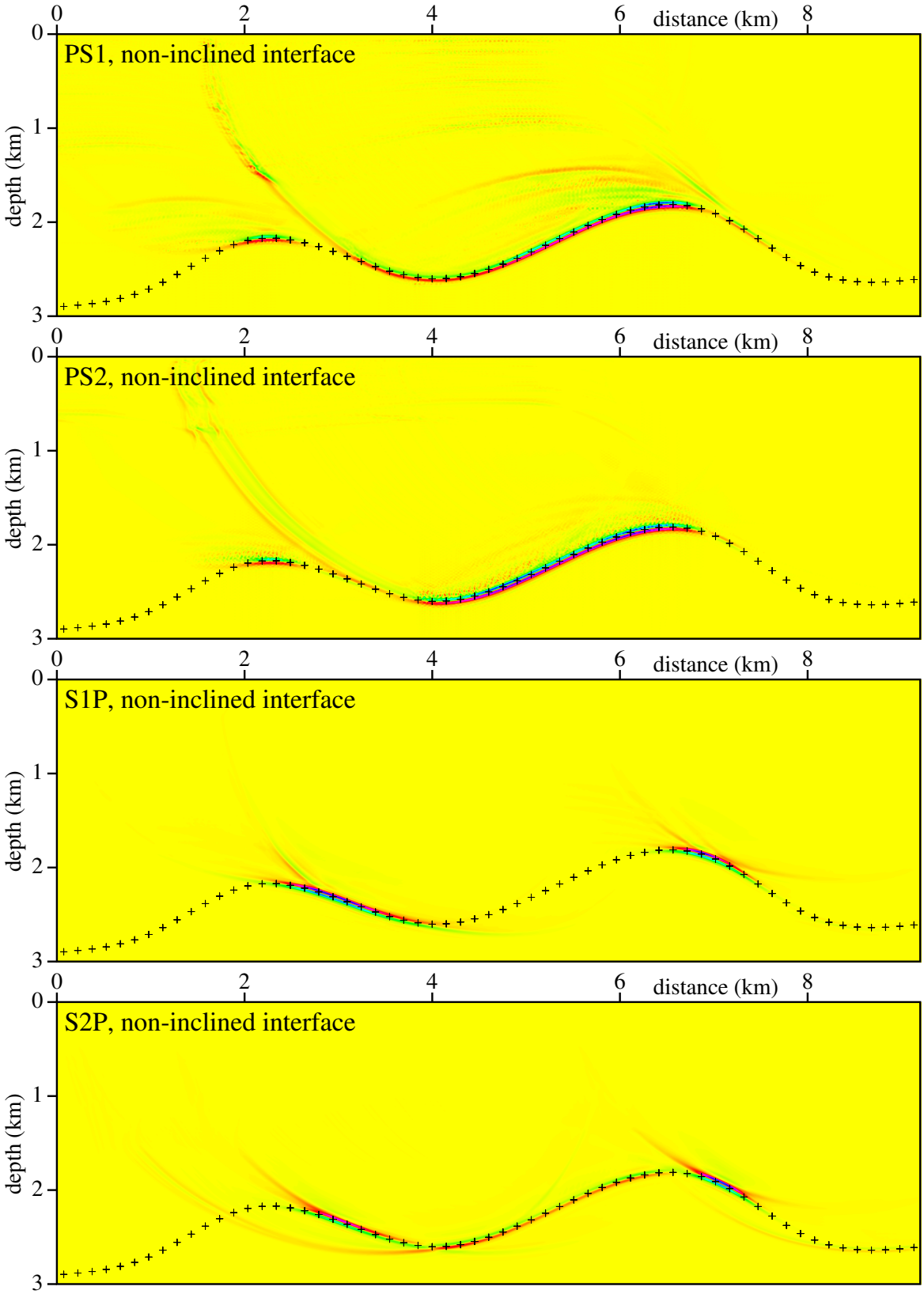

Figure 16. Stacked migrated sections calculated in the correct velocity model without interfaces specified by triclinic anisotropy. The PS1, PS2, S1P and S2P converted waves are used. The elastic moduli in the single-layer velocity model for migration are the same as in the upper layer of the velocity model used to calculate the recorded wave field. 81×240 common-shot prestack depth migrated sections, corresponding to 81 profile lines and 240 sources along each profile line, have been stacked. The crosses denote the interface in the velocity model used to compute the recorded wave field.

6. Conclusions

We generated synthetic seismograms of P, S and converted waves using the ray theory in a simple two-layer velocity model composed of two homogeneous layers with triclinic anisotropy in the upper layer. We then applied the 3-D ray-based Kirchhoff prestack depth migration to the correct homogeneous single-layer velocity model with the same triclinic anisotropy. We observed poorly imaged and noisy migrated sections for S and converted waves. The reasons are the use of only vertical component of seismograms and S wave singularities.

Acknowledgments

The author thanks Luděk Klimeš and Ivan Pšenčík for their help throughout the work on this paper. The research has been supported by the Grant Agency of the Czech Republic under Contract P210/10/0736, by the Ministry of Education of the Czech Republic within Research Projects MSM0021620860 and CzechGeo/EPOS LM2010008, and by the members of the consortium "Seismic Waves in Complex 3-D Structures" (see "http://sw3d.cz").

References

Bucha, V. (2012): Kirchhoff prestack depth migration in 3-D simple models: comparison of triclinic anisotropy with simpler anisotropies. *Stud. geophys. geod.*, **56**, 533–552.

Bucha, V. (2013): Kirchhoff prestack depth migration in velocity models with and without vertical gradients: Comparison of triclinic anisotropy with simpler anisotropies. In: *Seismic Waves in Complex 3-D Structures, Report 23*, pp. 45–59, Dep. Geophys., Charles Univ., Prague, online at "http://sw3d.cz".

Bucha, V. (2014): Kirchhoff prestack depth migration in triclinic velocity models with differently rotated tensors of elastic moduli. *Seismic Waves in Complex 3-D Structures*, **24**, 77–93, online at "http://sw3d.cz".

Bucha, V. & Bulant, P. (eds.) (2015): SW3D-CD-19 (DVD-ROM). *Seismic Waves in Complex 3-D Structures*, **25**, 209–210, online at "http://sw3d.cz".

Bulant, P. (1996): Two-point ray tracing in 3-D. *Pure appl. Geophys.*, **148**, 421–447.

Bulant, P. (1999): Two-point ray-tracing and controlled initial-value ray-tracing in 3-D heterogeneous block structures. *J. seism. Explor.*, **8**, 57–75.

Bulant, P. & Klimeš, L. (1999): Interpolation of ray-theory travel times within ray cells. *Geophys. J. int.*, **139**, 273–282.

Červený, V., Klimeš, L. & Pšenčík, I. (1988): Complete seismic-ray tracing in three-dimensional structures. In: Doornbos, D.J. (ed.), *Seismological Algorithms*, Academic Press, New York, pp. 89–168.

Gajewski, D. & Pšenčík, I. (1990): Vertical seismic profile synthetics by dynamic ray tracing in laterally varying layered anisotropic structures. *J. geophys. Res.*, **95B**, 11301–11315.

Klimeš, L. (2002): Relation of the wave-propagation metric tensor to the curvatures of the slowness and ray-velocity surfaces. *Stud. geophys. geod.*, **46**, 589–597.

Mensch, T. & Rasolofosaon, P. (1997): Elastic-wave velocities in anisotropic media of arbitrary symmetry-generalization of Thomsen's parameters ϵ, δ and γ. *Geophys. J. Int.*, **128**, 43–64.

Versteeg, R. J. & Grau, G. (eds.) (1991): The Marmousi experience. *Proc. EAGE workshop on Practical Aspects of Seismic Data Inversion (Copenhagen, 1990)*, Eur. Assoc. Explor. Geophysicists, Zeist.